Journal of Solar Energy Research (JSER)

Journal homepage: www.jser.ut.ac.ir

Numerical Investigation of Time-Dependent Dust Shading Effects on Fixed and Tracking Solar Photovoltaic Arrays

Kudzanayi Chiteka, C.C Enweremadu*

Department of Mechanical Engineering, University of South Africa, Science Campus, Florida 1710, South Africa

ARTICLE INFO

Article Type:

Research Article

Received:2026.01.28
Accepted in revised form:2026.04.09

Keywords:
Solar geometry dynamics;
Optical losses;
Thermal losses;
Diurnal shading;
Energy yield prediction;
Incidence angle effects

A B S T R A C T

The global expansion of solar energy has been met with dust soiling which is a critical performance-limiting factor, especially in dusty climates. The present study proposed a dynamic numerical approach for quantifying the time-dependent effects of dust shading on fixed-tilt, single-axis tracking, and dual-axis tracking PV systems. The approach was to distinguish between direct and diffuse irradiance and account for diurnal and seasonal solar geometry while incorporating angular-dependent shading dynamics. Single-axis and dual-axis trackers achieved daily yields of 5.02 kWh/day and 5.16 kWh/day respectively under a surface-soiling fraction of 32.7% determined from binary image segmentation and pixel-area ratio surpassing the clean fixed-tilt baseline of 4.41 kWh/day. A laboratory validation was used to confirm the ability of model to capture angular-dependent losses. A techno-economic analysis done revealed a trade-off where tracking systems maximise the absolute energy generated. However, fixed-tilt systems delivered superior cost-effectiveness due to lower capital and maintenance requirements. The results revealed the need for a dynamic, time-resolved model to improve optimisation and performance prediction, and guide maintenance strategies in soiling-prone environments.

1. Introduction

Solar photovoltaic (PV) systems play a critical role in the global energy transition toward low-carbon energy systems due to their environmental benefits and rapidly declining costs. The deployment of solar energy systems in residential, commercial, and utility-scale applications is accelerating worldwide, contributing to both climate change mitigation and enhanced energy security [1]. The efficiency and reliability of these PV systems are, however, influenced by several environmental and design

*Corresponding Author Email: enwercc@unisa.ac.za

Cite this article: Chiteka, K. and Enweremadu, C. (2026). Numerical Investigation of Time-Dependent Dust Shading Effects on Fixed and Tracking Solar Photovoltaic Arrays. Journal of Solar Energy Research, 11(2), 2934-2952. doi: 10.22059/jser.2026.410193.1709

DOI: 10.22059/jser.2026.410193.1709

parameters, including solar irradiance, installation geometry, temperature, soiling, and overall system configuration [2]. Exposure of PVs to environmental stressors increasingly affects long-term performance as these PV installations are expanding into a wide range of climates spanning from arid deserts to humid coastal and urban regions. Among these, soiling, which is the accumulation of airborne particulates on PV surfaces, has emerged as a globally recognised performance-limiting factor [3-5].

Empirical studies and simulation-based analyses have shown that soiling can reduce PV energy output by 5% to over 40% annually, depending on a range of factors including geographic location, atmospheric composition, environmental dust load, particle characteristics, panel design and orientation, and the frequency of cleaning. These losses often result in substantial operational and financial impacts, particularly for utility-scale PV systems, where even modest efficiency reductions translate into significant revenue loss over time [6,7]. For example, Al Garni [8] observed performance reductions from as little as 2% to over 50%, driven by site-specific dust characteristics and storm events in arid regions. Soiling is not confined to desert regions alone and even areas with frequent rainfall are also affected due to the deposition of pollution-related particulates and organic matter [9]. Field observations in Bangladesh have confirmed the severity of this issue and show that dust can block up to 55% of visible light in one month. As such, these observations indicate that weekly cleaning can recover approximately 3% of energy yield [10]. In another study, de Souza et al. [11] found that energy losses increased from 4.8% to 38.1% over five weeks depending on tilt and location. The financial impacts of soiling are significant and annual revenue losses can reach millions of dollars and this justifies the need for accurate, site-specific soiling models to guide operational decisions [12]. Moreover, the variability in soiling-induced degradation patterns between large-scale and small-scale PV systems calls for context-specific strategies, as highlighted by Cormode [13]. In a different environment, Pavan et al. [14] also reported annual soiling losses of about 6.9% at a utility-scale plant situated in Italy. This justifies the need for targeted cleaning strategies even in temperate climates.

Soiling usually affects PV performance primarily through optical attenuation mechanisms which include absorption, scattering, and reflection of incident light, and this is governed by the physical, chemical, and spatial characteristics of the deposited dust particles [15-17]. Darker, iron-rich dusts often exhibit higher absorptivity which leads to more severe transmittance losses, while lighter, silicate-based particles usually cause less attenuation due to their lower absorption coefficients [16,18]. The morphology and size of dust particles further influence attenuation with small particles (<45 μm) and soot-like aggregates which have fractal geometries significantly increasing scattering. This occurs especially at oblique angles of incidence, and form optically dense films that suppress transmittance across a broad spectral range [19-21]. Non-uniform dust deposition further compounds these optical effects leading to localised irradiance mismatches, hot spots, and a reduction in string-level efficiency. This particularly happens in large-scale installations exposed to heterogeneous environmental conditions [7,22]. Such spatial and temporal variability of soiling is often poorly captured in conventional performance models. These typically neglect the fine-scale interactions between particle properties, incidence angle, and module layout.

Module installation geometry plays a crucial role in modulating both soiling accumulation and angular losses. Steeper tilt angles promote gravitational removal of coarse particles but also expose the surface to higher angular losses during early morning and late afternoon hours, whereas shallower tilts tend to accumulate more dust due to reduced self-cleaning, yet benefit from lower optical attenuation near solar noon [23-25]. Dynamic PV tilt strategies seem to offer promising mitigation pathways. Dahlioui et al. [26] demonstrated that adjusting PV tilt angle from 30° at sunrise to 0° at sunset often reduce daily soiling by two-thirds. Khan et al. [27] showed that optimal PV tilt angles are strongly dependent on the latitude and seasonal variations, which justify the need for location-specific configurations. Studies have shown that azimuth orientation, in combination with tilt, also affects soiling rates and energy yield [28,29]. Nwokolo et al. [29] provided an empirical validation showing that optimised tilt angles not only reduce soiling but also significantly improve performance. Similarly, Feteh [30], highlighted the importance of optimised tilt strategies in maximising lifetime energy yield, demonstrating the comparative performance advantages of tracking systems under varying solar angles and seasonal shifts.

Solar tracking systems have been widely adopted particularly in large-scale PV installations to mitigate angular losses and optimise irradiance capture [31,32]. These tracking systems keep solar irradiance at normal incidence angles throughout the day by continuously adjusting panel orientation relative to incoming solar irradiance. Single-axis trackers work through correcting azimuthal alignment to the solar

irradiance while dual-axis trackers modify both azimuth and tilt angles to follow the sun's path [33]. Empirical reports have indicated that tracking systems can enhance energy harvest by 30 – 85% when compared to fixed-tilt arrays [34]. With regards to this, a study by Barbón et al. [33] showed that horizontal single-axis trackers delivered an 8.5% annual energy gain over fixed systems under real environmental conditions and the strongest gains occurred from March to September. Despite tracking systems having an angular optimisation advantage, they remain vulnerable to soiling because the continuously varying orientation introduces complex interactions between irradiance angles and dust shading geometry. Studies have revealed some mechanical challenges encountered in implementing reliable actuator designs for mobile tracking platforms, especially in dual-axis systems, which remain an underexplored area of research [35]. Abdulkarim [36] reported enhanced energy yield by approximately 30% in dual-axis trackers compared to fixed systems despite single-axis configurations providing a more favourable balance between cost, complexity, and performance. However, the benefits of tracking were found to diminish sharply under conditions of heavy soiling unless frequent cleaning regimes are employed [37]. Conventional static soiling correction approaches fail to capture the effects of dynamic orientation and uneven dust distribution. Some recent innovations such as the self-cleaning "NightFlip" tracker proposed by Pouladian-Kari et al. [38] and AI-enhanced dual-axis systems with nanocoatings proposed by Mamodiya et al. [39] offer promising solutions for mitigating soiling losses while enhancing adaptability and operational efficiency in diverse operating environments.

The dynamic interaction of dust with the solar incidence angle is a critical yet underexplored aspect of soiling, which varies continuously throughout the day and across seasons. The incidence angle of solar irradiance on the PV surface influences both the optical path length through the dust layer and the degree of scattering. Soiling losses therefore tend to be most severe at oblique incidence angles typically during early morning and late afternoon hours when the sun is low on the horizon and diffuse irradiance dominates [40]. A study by Chala et al. [41] reported that such angular effects led to power losses up to 18.8% in desert environments. Gedifew and Benor [23] also showed that dual-axis tracking systems significantly mitigate angular-dependent losses by maintaining near-normal incidence angles for longer durations and this achieves energy gains of up to 44.9% over fixed-tilt systems.

Regardless of these insights obtained from literature, most modelling approaches continue to represent soiling-induced shading as static or daily averaged phenomena, thereby overlooking the continuous diurnal variability of incidence-angle-dependent attenuation. Traditional models apply static or daily-averaged correction factors and fail to account for sub-daily variability, changing solar angles, and the interaction between diffuse radiation and angular transmittance [42]. Although there are growing insights into soiling mechanisms and their effects on PV performance, predictive models have mostly remained oversimplified and assume uniform soiling, neglecting the angular dependence of irradiance losses. For example, Pagani et al. [43] proposed a soiling index suitable for operational use, but it lacked temporal resolution thereby limiting its accuracy.

As a result, the temporal interaction between sun-path geometry, dust morphology, and irradiance partitioning into direct and diffuse components remains inadequately resolved within existing frameworks. Existing research generally treats soiling-induced shading as static or averaged phenomena, which leads to an incomplete understanding of diurnal soiling evolution under varying tracking and environmental conditions. Moreover, comparative studies which simultaneously quantify the combined impact of soiling and solar tracking geometry in fixed-tilt, single-axis, and dual-axis systems under identical environmental conditions remain limited in literature. This limitation constrains the development of robust cleaning schedules, tilt adjustment strategies, and tracking optimisation in dust-prone regions.

The present study seeks to address these limitations and develop a comprehensive numerical framework to explicitly model the time-dependent evolution of dust-induced shading on PV modules installed in fixed-tilt, single-axis, and dual-axis tracking configurations. The proposed approach enables sub-daily predictions of shading-induced transmittance losses and corresponding energy yield reductions through the integration of dynamic solar geometry, spectral-angular irradiance profiles, and dust layer characteristics. This approach allows for an improved representation of soiling interactions with changing solar incidence angles. This offers a step change from conventional static models toward a more physically grounded and temporally resolved performance analysis. This approach advances the scientific understanding of soiling–shading dynamics and their real-time impacts on PV performance by resolving the complex interplay between dust

morphology, incidence-angle variability and system geometry. The proposed framework captures the diurnal distribution of optical losses with more precision unlike the traditional models which overlook angular dependence and time-varying effects of soiling. The proposed framework therefore serves as both a diagnostic tool for performance degradation and a decision-support system for optimising cleaning schedules, tilt angle configurations, and tracking strategies in dust-prone regions.

2. Methodology

2.1. Simulation Framework

The simulation framework developed for this study employs MATLAB as the computational environment to implement the numerical analysis of dust-induced shading effects on PV systems. The simulation provided a platform to integrate solar geometry, parametric studies of PV array configurations, and time-series simulations which are essential for the modelling of the dynamic nature of soiling losses [44]. The study considered three main configurations commonly encountered in practice and these were fixed-tilt, single-axis tracking, and dual-axis tracking systems. The simulated PV system corresponds to a 1 kW array configuration, represented by two commercially available 500 W modules connected as a single string.

Fixed-tilt arrays were modelled with an inclination angle, β of 26°, which was selected as the latitude-based annual optimum for the study location (University of South Africa, Florida campus). Single-axis trackers were modelled and simulated as azimuth-tracking systems rotating about a vertical axis such that $\gamma(t) = \gamma_s(t)$ while maintaining a constant tilt β, where γ(t) and γ□(t) are respectively the array azimuth angle at time t and solar azimuth angle at time t. This was done to reduce the incidence-angle mismatch over the diurnal cycle. On the other hand, the dual-axis trackers were designed to continuously adjust both azimuth and elevation angles to maintain a near-normal solar incidence throughout the day.

Hourly meteorological data comprising the Direct Normal Irradiance (DNI), Diffuse Irradiance (DI), ambient temperature, and wind speed were obtained from January 2014 to December 2024 using the NASA POWER database (https://power.larc. nasa.gov/data-access-viewer/). The hourly DNI and DI values were averaged across all days of the year for each hour to construct an annual-mean representative diurnal cycle. The multi-year meteorological dataset was thus compressed into a single representative day profile for modelling purposes.

For every hour within the selected daylight analysis window from 05:00 - 18:00 hours local time, the solar position and module incidence angle were computed using Eqs. (1) - (3). The corresponding direct and diffuse shading areas were then computed from the projected shadow which in turn is dependent on the incidence angle (Eqs. (4) - (5)). Solar tracking affects the irradiance incidence angles and was incorporated in these computations, and the hourly energy output was computed cognisant of the resulting direct and diffuse shading-based energy formulations as shown in Eq. (8).

The analysis window was selected to capture the dominant daylight contribution in the annual-mean profile, and there was negligible irradiance outside this window. All comparisons made for the different configurations were therefore based on this annual-mean representative diurnal cycle instead of the 8760-hour year-by-year simulations.

2.2. Incidence Angle Modelling

The solar zenith angle, θ_z (Eq. (1)) and solar azimuth angle, γ□ (Eq. (2)) were calculated as functions of geographic latitude (ϕ), solar declination (δ), and hour angle (ω) using solar geometry relations.

$$cos\theta_z = sin\phi \cdot sin\delta + cos\phi \cdot cos\delta \cdot cos\omega \quad (1)$$

$$\gamma_s = arctan2(-\sin\omega, \tan\delta \cdot \cos\phi - \sin\phi \cdot \cos\omega) \quad (2)$$

$$cos(\theta_i) = \cos(\theta_z)\, cos(\beta) + sin(\theta_z)\, sin(\beta)\, co\, s(\gamma_s - \gamma) \quad (3)$$

The incidence angle (θ_i) on the tilted PV array was given by Eq. (3) where β and γ are respectively the tilt and azimuth angles of the array. The models resolve these quantities at hourly intervals from sunrise to sunset based on the annual-mean representative diurnal profile derived from the multi-year dataset.

2.3. Fixed-Tilt PV Array Model

The fixed-tilt model simulated arrays mounted at a constant tilt angle of β = 26°, based on the latitude-based annual optimum for the study location. The model used in the simulation distinguished between direct and diffuse shading effects. Direct shading occurs when dust particles block the direct beam component of solar irradiance. For a spherical dust particle of radius r, the projected area (A_g) onto the tilted module surface under an angle of incidence θ_i is given by:

$$A_g = \pi r^2 \cdot cos\theta_i = \pi r^2 \cdot cos\theta_z \cdot cos\beta + sin\theta_z \cdot sin\beta \cdot cos(\gamma_s - \gamma) \quad (4)$$

This angular dependence reflects the reduced shadow projection at oblique angles, especially during early morning and late afternoon periods. Diffuse shading (A_d) arises from elliptical shadows cast by dust particles under diffuse sky radiation. Assuming the dust particles form ellipsoidal projections due to oblique angles, the diffuse shaded area is expressed as:

$$A_{\mathrm{d}} = \pi ab = \frac{\pi r^2}{\cos\theta_i} \quad (5)$$

where $a = \frac{r}{\cos(\theta_i)}$ is the major axis and b = r is the minor axis of the ellipse.

Solar incidence angles have hourly variations, hence the direct (A_g) and diffuse (A_d) shaded areas were integrated over time. The total daily direct and diffuse shaded areas were obtained by integrating A_g and A_d from 05:00 to 18:00 hrs where $A_g(t)$ and $A_d(t)$ are the daily time-integrated shaded areas over daylight hours respectively for direct and diffuse shaded areas. t_5 and t_{18} are respectively the 5th and 18th hours of the day corresponding to local time 05:00 and 18:00 hrs.

$$A_g(t) = \int_{t_5}^{t_{18}} \left(\pi r^2 \cdot cos\theta_z \cdot cos\beta + sin\theta_z \cdot sin\beta \cdot cos(\gamma_s - \gamma)\right)(t) \cdot dt \quad (6)$$

$$A_{\mathrm{d}}(t) = \int_{t_5}^{t_{18}} \left(\frac{\pi r^2}{|\cos\theta_i|}\right)(t) \cdot dt \quad (7)$$

The instantaneous energy output, *E(t)*, accounting for shading was formulated as shown in Eq. (8),

$$E(t) = A.\left[(B_1).A_c - (B_2).n.A_g(t) - (B_2).n.A_d(t)\right] \quad (8)$$

where,

$A = P_{STC}.[1 + \kappa \times (T - T_{STC})]$, $B_1 = \left(\frac{G_{\mathrm{b}}(t)+G_d(t)}{G_{STC}}\right)$, and $B_2\left(\frac{G_{\mathrm{b}}(t)(1-T(\theta_i))}{G_{STC}}\right)$. n is the number of dust particles per unit area, A_c is the active array area and, α is the temperature coefficient. A is the temperature-adjusted power scaling factor based on the rated Standard Test Conditions (STC) maximum power (P_{STC}) and T is the operating module temperature. T_{STC} is the STC temperature taken as 25°C, and κ is the power temperature coefficient. The term B_1 is a dimensionless irradiance normalisation factor determined from the direct irradiance $G_b(t)$ and diffuse irradiance $G_d(t)$, normalised by the STC irradiance G_{STC} (1000Wm^2). B_2 is a beam-weighted, dimensionless loss term which accounts for optical/transmissivity effects dependent on the angle of incidence. $T(\theta_i)$ is the angular-dependent transmissivity function. The hourly conversion efficiency was computed as:

$$\eta(t) = \frac{E(t)}{A_c\, G_{POA}(t)\, \Delta t}, \quad (9)$$

where $G_{POA}(t) = G_b(t) + G_d(t)$ is the plane-of-array irradiance and Δt is the time step equal to 1 h. The daily-average conversion efficiency $\bar{\eta}$ was obtained by averaging $\eta(t)$ over the daylight hours, and the efficiency loss due to soiling was reported as:

$$\Delta\eta(\%) = \frac{\bar{\eta}_{clean} - \bar{\eta}_{soiled}}{\bar{\eta}_{clean}} \times 100\%. \quad (10)$$

where $\bar{\eta}_{clean}$ is the daily-averaged efficiency of the clean array and $\bar{\eta}_{soiled}$ is the daily-averaged efficiency of the soiled array. $\Delta\eta$ is the percentage efficiency reduction caused by soiling.

2.4. Single-Axis Tracking PV Model

In this configuration, the PV array was mounted on a vertical-axis azimuth-tracking system to maintain a constant tilt β while rotating in azimuth to satisfy $\gamma(t) = \gamma_s(t)$. The tracker used a constant tilt angle β while allowing the panel to rotate azimuthally throughout the day, following the sun's apparent motion from east to west. This rotation was meant to always ensure that the azimuthal offset ($\gamma s - \gamma$) = 0. This was done to reduce the incidence angle and enhance irradiance capture compared to fixed-tilt systems. Since $\gamma(t) = \gamma_s(t)$, the incidence angle simplifies to:

$$\cos\theta_i = \cos\theta_z \cos\beta + \sin\theta_z \sin\beta. \quad (11)$$

The projected dust shadow areas for direct and diffuse shading were thus expressed as:

$$A_g(t) = \pi r^2 \cos\theta_i\,(t), \quad (12)$$

$$A_d(t) = \frac{\pi r^2}{\cos\theta_i(t)}. \quad (13)$$

The total daily shading areas were computed by integrating over the daylight period:

$$A_g(t) = \int_{t_5}^{t_{18}} \pi r^2 \cos\theta_i\,(t)\,dt, \quad (14)$$

$$A_d(t) = \int_{t_5}^{t_{18}} \frac{\pi r^2}{|\cos\theta_i(t)|}\,dt. \quad (15)$$

The instantaneous energy output accounting for dust shading was then computed using Eq. (8).

2.5. Dual-Axis Tracking PV Model

The tracker of this configuration adjusts the tilt angle β and azimuth angle γ dynamically at every time step to ensure that $\theta_i(t) \approx 0°$ whenever the sun is above the horizon. This is done to maintain a near-normal incidence throughout the effective daylight period. As such, the cosine of the incidence angle simplifies to unity, $\cos\theta_i\,(t) = 1$. Since the irradiance incidence angle is minimised continuously, the shadow projection areas are simplified. For dual-axis tracking, $A_g(t) = A_d(t) = \pi r^2$. This shows the fact that the projected area of a spherical particle becomes constant under normal incidence, eliminating the angular dependence seen in the fixed and single-axis configurations. The total daily shading areas are integrated over the sunlight hours as,

$$A_g(t) = A_d(t) = \int_{t_5}^{t_{18}} \pi r^2\ dt \quad (16)$$

The instantaneous energy output was then determined using Eq. (8).

2.6. Optical - Electrical Coupling Framework

The optical model used in the study was first used to define an effective irradiance on the solar array by applying the direct and diffuse shading to the configuration-specific POA components as shown in Eq. (17). Here $G_{\text{eff}}(t) W/m^2$ is the effective POA irradiance incident on the PV array surface after soiling losses. The $G_{\text{eff}}(t)$ was obtained from the sum of the configuration-specific beam and diffuse POA components, $G_{b,\text{POA}}(t)$ and $G_{d,\text{POA}}(t)$, reduced by the corresponding fractional soiling attenuation terms $S_b(t) = min\left(1, \frac{n A_g(t)}{A_c}\right)$, is the fraction of beam POA blocked by particle geometric shadows and $S_d(t) = min\left(1, \frac{n A_d(t)}{A_c}\right)$ is the fraction of diffuse POA blocked. τ_{soil} is the residual transmittance of the unshaded area.

$$G_{\text{eff}}(t) = [G_{b,\text{POA}}(t)(1 - S_b(t)) + G_{d,\text{POA}}(t)(1 - S_d(t))]\tau_{\text{soil}}. \quad (17)$$

$G_{\text{eff}}(t)$ and the modelled cell temperature $T_c(t)$ were used to model a standard single-diode PV module to obtain I_{mp}, V_{mp}, and P_{mp} for the three configurations under clean and soiled conditions. The differences in these electrical parameters therefore emanate from configuration-dependent POA irradiance and incidence angle under identical meteorological forcing, rather than changes in deposited dust coverage. In this study, τ_{soil} was taken as a controlled reference parameter and this was consistent with the silica-based dust used in the laboratory experiments. The geometric shadow projection terms $A_g(t)$ and $A_d(t)$, and the dust-layer transmittance factors were treated as complementary attenuation mechanisms. The former accounted for the direct particle-induced occlusion of incident irradiance, and the latter represents partial optical attenuation within the unshaded surface area, which avoids double accounting of losses.

2.7. Experimental Validation

Validation was achieved through a controlled laboratory experiment conducted using a solar simulator and monocrystalline PV cells (Figure 1), done in a single day. The validation had repeated measurements taken at each inclination angle for both clean and soiled cells under identical irradiance and ambient conditions.

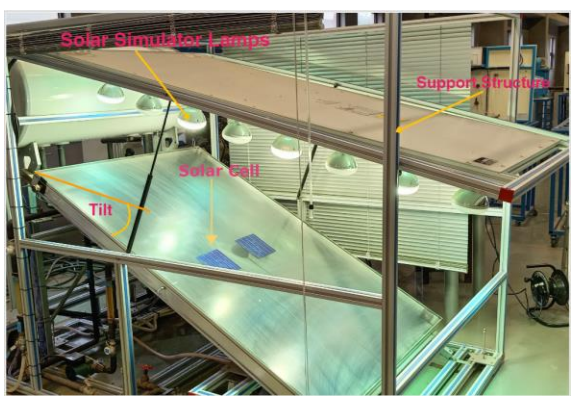

Figure 1. Experimental laboratory validation with solar simulator

This experimental validation was designed to replicate key conditions represented in the model under controlled settings. It eliminated environmental variability and allowed for systematic evaluation of

dust-induced shading effects. Uniform layers of silica-based dust particles with an average size distribution of 30 µm were deposited on the surface of PV test cells. After deposition, the geometric soiling fraction was quantified experimentally using image-based area analysis through binary segmentation and pixel-area ratio from the top-view images. Here, the geometric soiling fraction refers to the top-view fractional area of the cell surface occupied by particles and not the projected optical shadow fraction at operating incidence angles. This procedure yielded a measured uniform soiling fraction of 32.7%, which was adopted as the reference 'uniform soiling' condition in both the experiment and the numerical simulations. While this value represents a substantial geometric surface coverage, it was selected as a controlled, moderate-to-high reference condition for mechanistic evaluation rather than as a climatological average for the study location. It is important to note that this 32.7% value is a geometric top-view surface soiling fraction, and the effective irradiance penalty in the model was governed by the shadow projection based on the incidence angle, and dust-layer transmittance. Therefore, this surface soiling fraction does not translate linearly into an equivalent percentage energy loss.

The PV cells were mounted on a tilting platform beneath a calibrated and computerised solar simulator capable of providing and recording irradiance across the cell surface. The incident irradiance levels were monitored and recorded throughout the experimental process using the inbuilt pyranometer. In addition, an infrared camera was used to monitor cell temperature. Tests were only conducted once the incoming irradiance stabilised to maintain identical forcing conditions for the clean and dust-covered cases. The experimental procedure involved varying the tilt of the PV cell to simulate a range of solar incidence angles from normal incidence (0°) to highly oblique angles up to about 85°, to mimic the diurnal solar paths. At each inclination angle, power output measurements were made for both clean and dust-covered cells under identical irradiance and ambient conditions. The power output from the PV cells was derived using a PV analyser which measured the full I-V curve and reported P_{mp}, V_{mp}, and I_{mp} at each test condition. The data collected was used to provide a basis for comparison between predicted and experimentally observed reductions in PV output due to dust-induced shading.

2.8. Assumptions and Limitations

The modelling framework and laboratory-based validation presented in this study relied on simplifying assumptions. The model assumed that dust particles are perfectly spherical, homogeneous in size and composition, and uniformly distributed across the PV module surface. This idealisation allowed for analytical formulation of shadow projection areas but does not capture the diversity of particle morphologies, mineralogies, and deposition patterns observed under real-world conditions, where dust can be irregular, clustered, or exhibit spatial nonuniformity due to environmental factors. In contrast, actual PV installations often experience heterogeneous soiling patterns resulting from wind-driven deposition, rain streaking, or microclimatic effects that can produce localised hot spots and nonuniform performance degradation. The model further assumed a single static dust layer throughout each simulation period, neglecting time-dependent processes such as continuous deposition, resuspension by wind, and removal by precipitation, all of which dynamically influence soiling severity and recovery in field conditions.

The material and optical properties of dust were treated as constant, with no allowance for variations due to humidity, particle agglomeration, or surface cementation effects. These variations can modify the interaction between dust and incident light. Thermal conditions were assumed to be homogeneous across the PV module surface, and the temperature was modelled as uniform and independent of localised irradiance mismatches or shading-induced hot-spot effects. While the laboratory validation experiments were designed to isolate angular-dependent shading effects under controlled conditions, they simplified the complexity of outdoor environments. Moreover, they do not replicate the full range of dust compositions, deposition patterns, or environmental interactions encountered in field deployments.

To incorporate transmittance losses due to dust deposition into the numerical model, an average transmittance value (τ_{soil}) of approximately 0.85 was applied for silica-based dust layers reflecting partial attenuation from both absorption and scattering effects. This value was selected as a moderate baseline consistent with measured 10 - 20% reduction in transmittance under laboratory-controlled dust deposition conditions [16,45]. This was based on literature findings indicating that dust layers composed predominantly of silica can reduce transmittance by 10–20% depending on thickness and composition [46,47].

An uncertainty check was applied to the dominant uncertain inputs in the model to ascertain the impact of the simplifying assumptions on the reported performance metrics. The concerned metrics include the representative POA irradiance forcing, the estimated module temperature, and the optical soiling terms, which are geometric soiling fraction and the assumed dust-layer transmittance τ_{soil}. These inputs were perturbed within reasonable bounds and the resulting spread in the daily energy produced was examined to confirm that the main comparative conclusion that the energy from fixed-tilt is less than single-axis also less than dual-axis under identical forcing, is robust and not a result of a single-point assumption set.

3. Results and Discussion

3.1. Time-Resolved Analysis of Direct and Diffuse Shading Profiles

The dynamic characteristics of dust-induced shading were examined for the three configurations using time-resolved profiles of direct shading as shown in Figure 2(a). Hour 5 is the first daylight hour in the annual-mean representative diurnal profile. The shading fraction was determined at an hourly time step using the same formulations derived in Section 2. The values shown at hour 5 corresponds to the early-morning period when solar elevation is still low and incidence angles are still highly oblique. This eventually result in a larger effective shadow than around solar noon. This is simply because steep solar incidence angles magnify the effective shadow area cast by dust particles. Such behaviour highlights a fundamental limitation of fixed-tilt designs. They are unable to adapt orientation results in shading losses that accumulate over critical daily periods. This leads to a significant reduction in energy yield despite midday stability.

Single-axis tracking systems revealed a noticeable improvement in energy generation. They reduced direct shading substantially around midday, when solar irradiance is highest due to the continuous azimuthal adjustment. This reduces the angular mismatch between the irradiance and the module surface thereby mitigating shading during peak hours. However, single-axis systems showed some vulnerabilities during early morning and evening hours revealing their partial although not complete effectiveness.

Dual-axis tracking on the other hand presented the most favourable performance. This configuration effectively minimised angular amplification of shading. It maintained a near-constant projected shading area but energy losses from scattering and transmittance loss were still evident.

The strong angular dependence shown in the direct shading profiles in Figure 2(a) was consistent with recent findings. Studies show that soiling losses tend to increase significantly at oblique incidence angles due to enhanced geometric shading and scattering effects. This was in agreement with Guo and Javed [40] who reported that PV soiling losses increase with incidence angle. They indicated that soiling losses follow a clear angular amplification following a sec(θ)-type relationship.

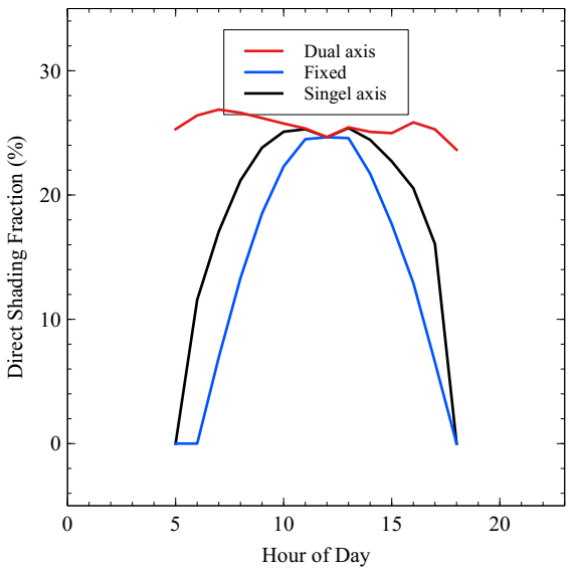

(a)

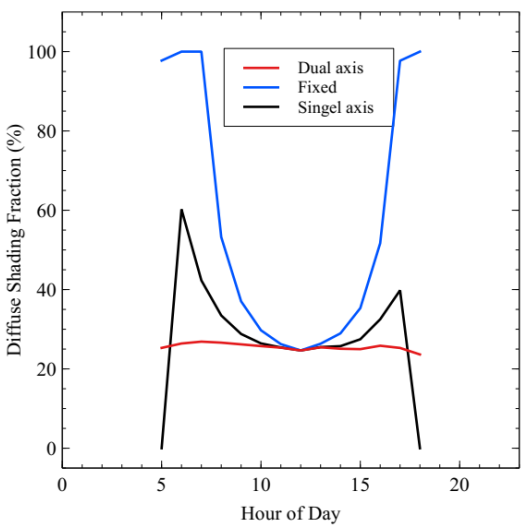

(b)

Figure 2. Hourly variation of (a) direct shading fraction (b) diffuse shading fraction, reflecting differences in angular alignment throughout the day

Figure 2(b) illustrates the diffuse shading profiles showing that the differences among the three configurations were comparatively minor compared to direct shading. This behaviour emanates from the fact that diffuse irradiance is scattered across a broad range of sky angles. The multidirectional arrival characteristic of diffuse irradiance mean that even advanced tracking systems cannot fully align modules to mitigate their shading effects. This reduces the influence of orientation compared to direct irradiance. Although this was the case, some advantages were still noticeable. Both single-axis and dual-axis tracking configurations exhibited marginal reductions in diffuse shading, particularly during midday when irradiance levels are highest. Their orientations which are meant for direct beam capture can partially reduce angular mismatches with diffuse irradiance. It can therefore be shown that although orientation cannot eliminate diffuse shading, it can slightly moderate its impact during peak periods of energy generation. Therefore, the benefits of solar tracking are more pronounced for direct shading with limited impact for diffuse shading

3.2. Energy Performance of Different Configurations Under Soiling Conditions

The simulated ideal clean 1kW PV array under fixed-tilt configuration produced about 4.41 kWh/day based on the annual-mean representative diurnal profile. This served as the baseline for evaluating performance across all the other different types of configurations. The reported 4.41 kWh/day represent the energy generation integrated over the annual-mean representative diurnal profile. The single-axis tracking system showed an improved energy output by about 20%, with approximately 5.29 kWh/day. This improved generation is attributed to its reduced incidence angles which enhances the direct irradiance capture. The dual-axis tracking configuration, on the other hand, showed the highest performance by yielding about 5.74 kWh/day, which was almost 30% increase in energy generated compared to the fixed-tilt configuration. These tracking-related yield improvements were found to be consistent with results reported in literature for tracking systems relative to fixed-tilt arrays under comparable irradiance conditions [31,48]. The energy improvements reported in the present study were moderate because the analysis was based on an annual-mean representative diurnal profile.

Table 1. Daylight-averaged MPPT electrical variables for the simulated 1 kW PV string (series connection) under clean and soiled conditions across three configurations

	Configuration	$\bar{E}_{day}$ (kWh/day)	$\bar{P}_{mp}$ (W)	$\bar{V}_{mp}$ (V)	$\bar{I}_{mp}$ (A)
Clean	Fixed-tilt	4.41	339.23	65.80	5.16
	Single-axis	5.29	406.92	65.80	6.18
	Dual-axis	5.74	441.54	65.80	6.71
Soiled	Fixed-tilt	4.28	329.23	65.47	5.03
	Single-axis	5.02	386.15	65.47	5.90
	Dual-axis	5.16	396.92	65.47	6.06

Table 1 provides the daily averaged maximum power point tracking (MPPT) electrical performance metrics for the simulated PV string under clean and soiled conditions for the three configurations. The table outlines the reported daily averaged energy yield ($\bar{E}_{day}$), maximum-power-point power ($\bar{P}_{mp}$), voltage ($\bar{V}_{mp}$), and current ($\bar{I}_{mp}$). These metrics provide a comparative analysis of the electrical representation of the tracking and soiling effects from the coupled optical–electrical framework. Although this is a 48 V nominal system, the MPPT metrics in Table 1 were reported on the PV-string side. The system was made up of 2 x 500 W modules with electrical parameters presented in Table 2. The modules were connected in series and the array operated near $V_{mp} \approx 2 \times 32.96 \approx 65.9$ V. The effective irradiance from the optical attenuation model was mapped to photocurrent in the single-diode ($I_{ph} \propto G_{eff}$), to translate the soiling-induced optical losses into electrical performance metrics.

Table 2. Electrical parameters of the used solar PV modules

Parameter	Symbol	Value
1	P_{max}	500 W
2	V_{mp}	32.96 V
3	I_{mp}	15.17 A

4	V_{oc}	38.60 V
5	I_{sc}	15.81 A
6	$\gamma_{P_{max}}$	−0.26 %/°C
7	$\beta_{V_{oc}}$	−0.24 %/°C
8	$\alpha_{I_{sc}}$	0.046 %/°C

Table 1 shows that the daylight-averaged power ($\bar{P}_{mp}$) increased with tracking under clean conditions. $\bar{P}_{mp}$ increased from 339.23 W in a fixed tilt configuration to 406.92 W and 441.54 W respectively in single- and dual-axis tracking. Under soiling conditions, the corresponding MPPT power decreased to 329.23 W, 386.15 W, and 396.92 W respectively. This reduction was derived from the averaged operating current which dropped from 6.71 - 5.16 A for the clean configurations to 6.06 - 5.03 A for the soiled configurations. The reduction in the operating current confirmed that dust-induced optical losses is shown as photocurrent penalty. The operating voltage in all the configurations for both clean and soiled modules remained nearly constant ($\bar{V}_{mp} \approx$ 65.8 V and 65.47 V) respectively for clean and soiled modules. The performance gap was therefore governed mainly by current and not the voltage. This is because soiling normally attenuates the effective irradiance G_{eff}, which reduces the light-generated current ($I_{ph} \propto G_{\text{eff}}$) almost linearly and MPP voltage is only weakly dependent on irradiance and is therefore generally less sensitive to moderate optical losses.

3.2.1. Fixed-Tilt PV Configuration

The simulated uniform soiling with geometric fractional coverage of about 32.7% decreased the energy of the simulated clean array from 4.41 to 4.28 kWh/day which was a percentage loss of about 2.95%. This relatively modest loss is expected because the 32.7% value represents a top-view geometric fractional shading and does not translate linearly into an equivalent diurnal beam-occlusion fraction. This is because projected particle shadows contract near solar noon under near-normal incidence, and diffuse irradiance is less sensitive to orientation. Furthermore, the adopted silica-based dust transmittance, τ of 0.85 represents partial attenuation of the unshaded surface rather than complete optical blockage.

Although the reported loss was lower than values often reported in desert environments, published field studies indicate a wide variability depending on dust composition, deposition characteristics, and angular effects. For example, Pavan et al. [14] reported annual losses of about 6.9% in temperate climates, whereas Chala et al. [41] and Al Garni [8] observed substantially higher reductions of up to 18 - 50% in arid regions associated with darker and more cohesive dust layers. In the present study dominated by silica dust, uniformly distributed fractional coverage shows a controlled moderate-to-high optical scenario, and the resolved angular-shading formulation explains why geometric shading does not translate directly to proportional energy loss.

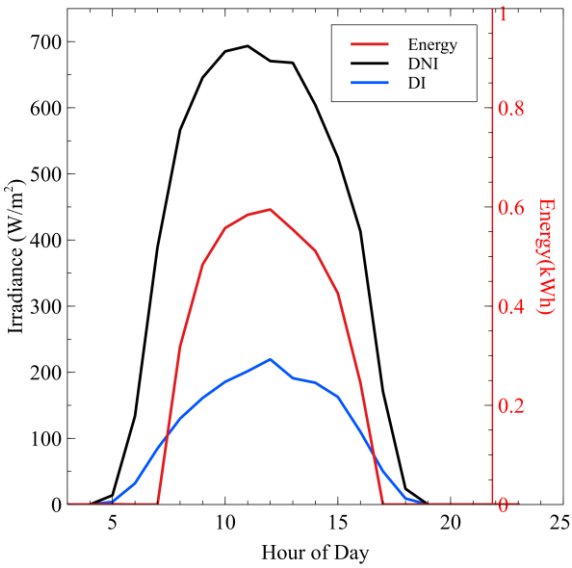

Figure 3. Diurnal profiles of direct normal irradiance (DNI), diffuse irradiance (DI), and hourly energy output (kWh) from a 1 kW fixed-tilt PV system under soiling conditions (Δt = 1 h)

Figure 3 shows the diurnal profiles of the DNI, DI, and PV system energy output. The DNI curve peaks sharply around midday, showing the strong directional component of solar radiation, while the DI curve is broader and less intense due to scattering in the atmosphere. The PV output profile closely follows these irradiance patterns but consistently lags in magnitude. This indicate both inherent conversion efficiency limits and the added influence of soiling and suboptimal incidence angles. Of note is the energy output curve which rises later in the morning and falls earlier in the evening than the irradiance curves. This reveals the fixed-tilt system reduced capacity to capture low-angle sunlight in the early morning and late afternoon. The observed diurnal mismatch illustrates why tracking systems can outperform fixed-tilt designs under identical soiling conditions. This is achieved by their capability to maintain favourable orientations particularly during morning and evening periods.

3.2.2. Single-Axis Tracking PV Configuration

Under the same uniform soiling conditions, the single-axis tracking system achieved a daily energy yield of about 5.02 kWh/day, surpassing even the ideal clean fixed-tilt system, which produced 4.41 kWh/day. At first glance, this outcome may appear counterintuitive given the perceived extent of fractional dust coverage. However, it illustrates the inherent strength of tracking technologies which minimises shading losses dependent on incidence angle. This dynamic alignment ensures more favourable exposure to incoming solar radiation. This substantially mitigates the negative impacts of dust particles when compared to the static geometry of fixed-tilt arrays.

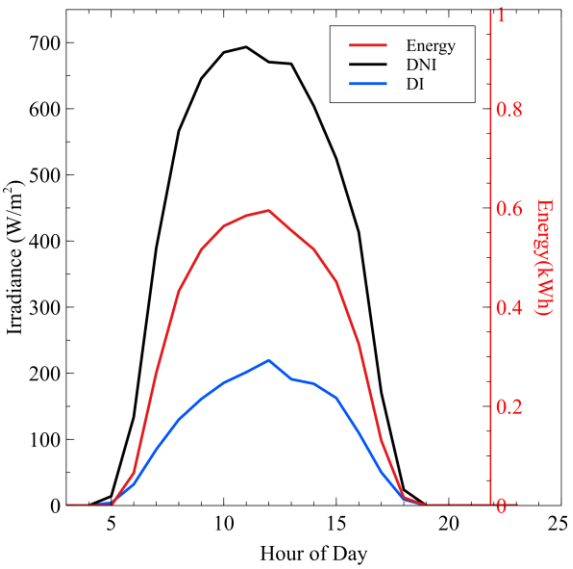

Figure 4. Diurnal profiles of direct normal irradiance (DNI), diffuse irradiance (DI), and hourly energy output (kWh) from a 1 kW single-axis tracking PV system under soiling conditions ($\Delta t = 1$ h)

Under identical irradiance conditions shown in Figure 4, the single-axis tracker extended productive hours compared to the fixed-tilt configurations by reducing incidence-angle penalties during morning and evening periods. The fixed-tilt energy output generally followed these trends but was consistently impacted by conversion losses and dust shading. As such, generation begins later in the morning and ends earlier in the evening, indicating the system's limited ability to capture oblique-angle sunlight. In contrast, the single-axis tracker extended the productive hours of energy generation by maintaining more favourable orientation throughout the day. This capability not only reduced the relative penalty of soiling but also allowed the system to outperform the clean fixed-tilt reference.

3.2.3. Dual-Axis Tracking PV Configuration

The dual-axis tracking system is capable of continuously adjusting both the tilt and azimuth angles. It delivered the highest energy yield under uniform soiling conditions, producing approximately 5.16 kWh/day. This output exceeds both the soiled fixed-tilt system (4.28 kWh/day) and the soiled single-axis tracker (5.02 kWh/day). The superior performance could be attributed to the elimination of incidence-angle–dependent shadow amplification in the geometric beam component ($\cos\theta_i = 1$). This leads to a constant projected particle area, while diffuse and transmittance-related losses retain their inherent diurnal dependence.

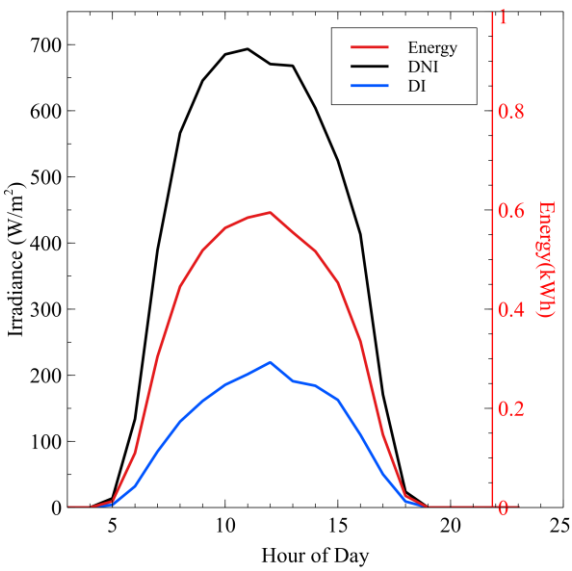

Figure 5. Diurnal variation of direct normal irradiance (DNI), diffuse irradiance (DI), and energy output from a soiled dual-axis tracking PV system

When compared to both fixed-tilt and single-axis systems, the dual-axis tracker (Figure 5) maintained a near-normal alignment between the PV array and the solar irradiance throughout the day. This had an effect of widening the effective energy production window during the day. The output curve of the dual-axis system closely mirrors the irradiance profiles but demonstrates superior temporal consistency. The dual-axis system exhibited higher output even during low-solar-elevation morning and late-afternoon hours compared to both fixed-tilt and single-axis systems. This extended energy generation reflects improved alignment with the direct beam irradiance

component, while diffuse irradiance remained comparatively less sensitive to the array geometry.

The operational efficiency of the three configurations was averaged over the daylight hours of the annual-mean representative diurnal profile. These operational efficiencies were found to be approximately 22.45% for the fixed-tilt and respectively 21.95% and 20.80% for the single-axis and dual-axis configurations. This corresponds to relative efficiency losses of 2.95%, 5.10%, and 10.10%, respectively. It is important to note that these are configuration-dependent operational efficiencies defined with respect to $G_{POA}(t)$. Furthermore, the angular or soiling penalties, and the intrinsic STC module conversion efficiency of 23.13% were treated as a fixed reference electrical baseline.

It is also important to recognise that the technical gains of tracking were not without trade-offs. Dual-axis trackers are associated with higher capital investments, increased mechanical complexity, and more intensive maintenance requirements. In dusty or remote environments, where servicing and cleaning schedules may already be constrained, these demands can present additional operational challenges. Thus, while dual-axis systems clearly maximise daily yield and minimise shading-induced losses, their practical deployment requires a balanced evaluation of performance benefits versus economic and logistical realities. For many applications, especially in resource-limited settings, the decision may hinge not only on maximising technical output but also on ensuring long-term reliability and manageable lifecycle costs.

3.3. Comparative Energy Yields Across PV Configurations

Figure 6 summarises the daily energy yields of the different configurations together with an experimentally measured result for a dust-covered fixed-tilt array. The results highlight the distinct performance hierarchy across configurations and the pronounced benefits of solar tracking technologies. Under clean conditions, tracking systems were found to substantially outperformed the fixed-tilt baseline. The experimental fixed-tilt energy of 3.65 kWh/day diverged significantly from the simulated soiled fixed-tilt value (4.28 kWh/day). This lower output indicates additional practical losses which are inherent in laboratory conditions. Such losses include optical non-idealities, spectrum mismatch of the solar simulator, minor electrical losses, and unavoidable micro-scale non-uniformities in dust deposition that are not explicitly resolved in the idealised uniform-coverage numerical model. The numerical model, instead, isolates angular-dependent shading under controlled geometric assumptions. This represents an idealised upper-bound estimate under identical fractional soiling conditions. The experimental value can therefore be interpreted as a lower-bound benchmark that validates the numerical model while highlighting the additional complexity of real-world conditions.

Figure 7 provides further insights by comparing the diurnal profiles of DNI, diffuse irradiance DI, and hourly energy output across the three soiled configurations. The dual-axis tracker produced the highest hourly energy yield by maintaining optimal alignment throughout the day. The single-axis tracker on the other hand, also performed strongly but showed reduced effectiveness during the early morning and late afternoon, when tilt misalignment limited its capture of low-angle sunlight. In contrast, the fixed-tilt array, which is constrained by its static orientation, delayed the energy generation in the morning and ceased earlier in the evening. This revealed its inability to adapt to changing solar geometry.

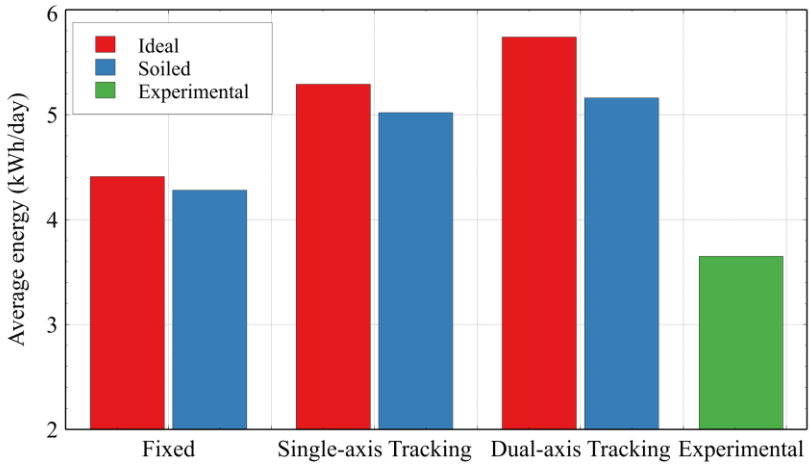

Figure 6. Daily energy output for six PV configurations, showing ideal and soiled conditions for fixed-tilt, single-axis tracking, and dual-axis tracking systems

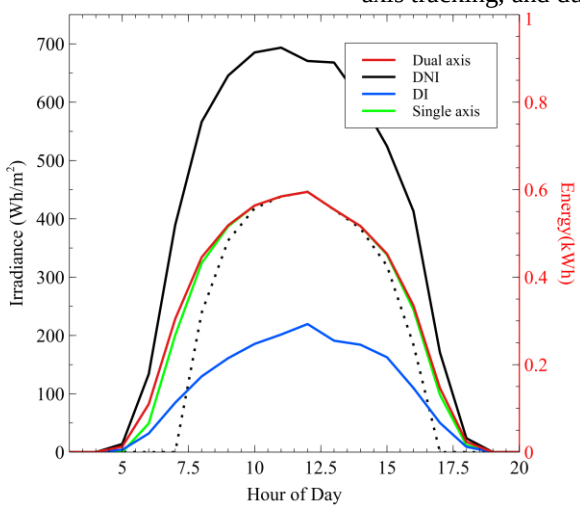

Figure 7. Diurnal profiles of DNI, DI, and energy output from different configurations under soiling conditions

The results from the present study demonstrated some critical points. First, tracking systems not only enhance performance under clean conditions but also sustain substantial yield advantages under soiling. Moreover, the time-varying incidence angle alters the effective projected shading which partially mitigates the expected transmittance-driven losses. This yields energy reductions in soiled fixed-tilt output which are smaller than expected.

3.4. Techno-economic Performance Evaluation

A techno-economic analysis was performed to evaluate the comparative performance and cost-effectiveness of the seven configurations. The analysis was based on a standard 500 W solar module used in the present study. The market-aligned costs were taken as follows; US$150 for the panel, US$30 for a fixed-tilt mount, US$100 for a single-axis tracker, and US$200 for a dual-axis tracker. Accordingly, the estimated capital expenditures (CAPEX) were US$180 for fixed-tilt, US$250 for single-axis, and US$350 for dual-axis configurations (See table 3 and Figure 8).

Table 3. Daily energy yield, capital expenditure (CAPEX), and energy-per-dollar performance (kWh/day/US$) for seven PV system configurations under ideal, soiled, and experimental conditions

Configuration	Daily Energy (kWh)	CAPEX (US$)	kWh/day/US$
Ideal fixed-tilt	4.41	180	0.0245
Ideal single-axis	5.29	250	0.0212
Ideal dual-axis	5.74	350	0.0164
Soiled fixed-tilt	4.28	180	0.0238
Soiled single-axis	5.02	250	0.0201
Soiled dual-axis	5.16	350	0.0147
Experimental fixed-tilt	3.65	180	0.0203

Table 4. Levelised cost of energy (LCOE) for seven PV system configurations over a 25-year lifetime, incorporating capital expenditure (CAPEX), discounted operation and maintenance (O&M) costs, and discounted lifetime energy yields

Configuration	Daily Energy (kWh)	CAPEX (US$)	O&M rate (%CAPEX/yr)	PV Energy (kWh, discounted over 25y)	PV Costs (US$, discounted)	LCOE (US$/kWh)
Ideal fixed-tilt	4.41	180	1.0	16497.6	199.21	0.0121
Soiled fixed-tilt	4.28	180	1.0	16011.3	199.21	0.0124
Experimental fixed-tilt	3.65	180	1.0	13654.5	199.21	0.0146
Ideal single-axis	5.29	250	1.5	19789.6	290.03	0.0147
Soiled single-axis	5.02	250	1.5	18779.6	290.03	0.0154
Ideal dual-axis	5.74	350	2.0	21473.1	424.72	0.0198
Soiled dual-axis	5.16	350	2.0	19303.3	424.72	0.022

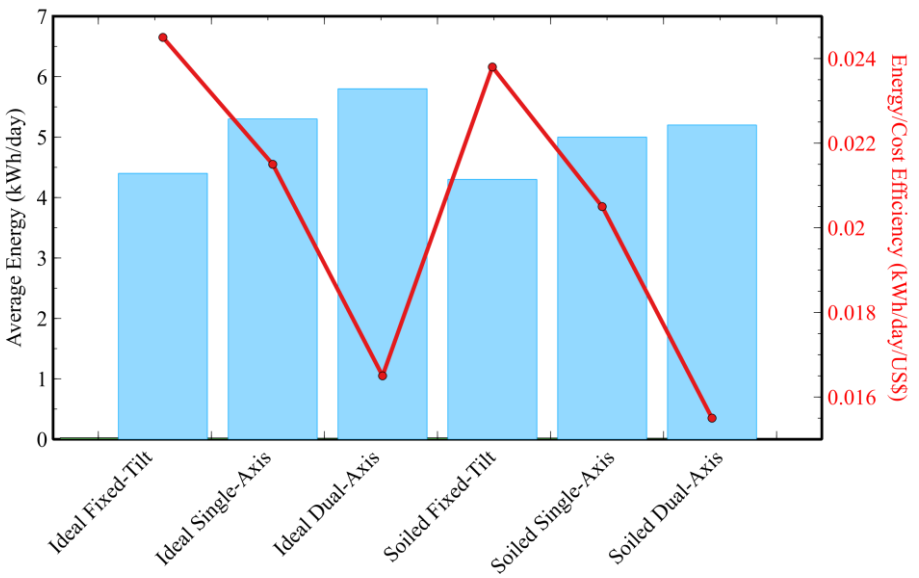

Figure 8. Comparison of daily energy output (blue bars, left axis) and cost-efficiency (red line, right axis) across different PV system configurations under ideal and soiled conditions

The fixed-tilt configuration reported the highest cost efficiency of 0.0245 kWh/day/US$ under clean conditions and 0.0238 kWh/day/US$ under soiling when assessed in terms of energy-per-dollar invested. The experimental fixed-tilt case had a cost efficiency of 0.0203 kWh/day/US$ which outperformed both single- and dual-axis tracking systems on this metric. In contrast, while tracking systems were technically superior in absolute energy generation, they exhibited lower cost efficiency due to their higher CAPEX, with dual-axis tracking recording the lowest values in the range 0.0147 - 0.0164 kWh/day/US$. When benchmarked against a reference electricity tariff of US$0.10/kWh, daily revenue potential ranged from US$0.36/day for the experimental fixed-tilt system to US$0.57/day for the ideal dual-axis tracker. Despite the latter's revenue advantage, fixed-tilt systems offered shorter simple payback periods because of their lower upfront investment and higher energy-per-dollar ratios.

Table 4 presents the levelized Cost of Energy (LCOE) for the different configurations. The results revealed a clear performance–cost trade-off in which fixed-tilt systems emerged as the most cost-effective, with LCOE values in the range US$0.0121 - 0.0124/kWh under clean and soiled conditions. Even the experimental fixed-tilt configuration, which delivered lower output due to dense laboratory dust coverage, achieved an LCOE of US$0.0146/kWh, which is still competitive in comparison to tracking

systems. Single-axis trackers on one hand achieved higher absolute energy yields. However, this came at the expense of higher capital and Operation and Maintenance (O&M) costs which raising their LCOE to US$0.0147 - 0.0154/kWh. Dual-axis systems exhibited the highest LCOEs ranging from US$0.0198 - 0.0220/kWh due to their high cost despite being technically superior in terms of daily output. These findings underscore a fundamental trade-off in which tracking maximises energy generation, while fixed-tilt maximises cost-efficiency. Under the controlled modelling assumptions and comparative energy estimates adopted in this study, fixed-tilt systems provided the strongest economic case in dust-prone regions, while tracking systems may still be justified where maximising yield is prioritised over minimising unit energy cost. It should be noted that the techno-economic evaluation presented here was intended as a comparative decision-support analysis under controlled cost assumptions rather than a full discounted cash-flow feasibility assessment. Parameters such as discount rate variation, tracker maintenance escalation under severe dust exposure, and dynamic cleaning costs were not explicitly varied in this framework. The primary objective was to evaluate relative performance-cost trade-offs across configurations under identical modelling conditions. Accordingly, the reported payback and LCOE metrics should be interpreted as indicative comparisons rather than site-specific investment forecasts.

3.5. Limitations, Recommendations, and Implications for PV System Design in Dusty Environments

The limitations identified in this study provide a roadmap for future research directions. The current numerical framework may be improved by the integration of dynamic environmental processes. These include time-varying dust deposition, wind-driven resuspension, and precipitation-induced cleaning effects which will reflect the evolving nature of soiling in real-world settings. Moreover, incorporating transient atmospheric conditions and spatially resolved thermal effects would improve the predictive realism and operational relevance of future models. Field validation which considers the heterogeneous nature of dust properties and varying climatic conditions are also critical to strengthen the applicability of the findings.

In addition to these recommendations, the findings bear some important practical implications for PV system design, particularly in dusty environments. The comparative analysis demonstrated that dynamic solar tracking systems substantially mitigate the adverse effects of dust-induced shading and achieved up to 30% energy yield improvements over static installations, even under considerable soiling conditions. This reinforces the strategic advantage of tracking technologies in regions prone to dust accumulation.

However, the adoption of tracking systems requires some considerations with regards to the trade-offs. These include higher capital costs, mechanical complexity, and increased maintenance demands. Single-axis trackers emerge as a promising compromise, offering significant performance gains over fixed-tilt systems while avoiding the higher costs and operational intricacies associated with dual-axis trackers. As such, system designers and operators must balance technical performance with site-specific economic, operational, and logistical factors when selecting an appropriate configuration.

4. Conclusions

The present study developed and validated a comprehensive numerical framework to evaluate the time-dependent impacts of dust-induced shading. Three different configurations including fixed-tilt, single-axis tracking, and dual-axis tracking were evaluated and analysed. The developed the model provided a realistic assessment of soiling losses than conventional static approaches. This was achieved through explicitly resolving diurnal variations in incidence angles and distinguishing between direct and diffuse irradiance. It should be emphasised that the framework isolates incidence-angle-dependent optical shading under controlled uniform coverage conditions. As such, it does not explicitly resolve cell-level mismatch, bypass diode activation, or spatially heterogeneous deposition patterns encountered in field environments. Accordingly, the results should be interpreted as mechanistic upper-bound performance comparisons under uniform soiling assumptions, rather than direct predictions of heterogeneous field degradation. Laboratory experiments under controlled dust coverage confirmed the ability of this framework to capture angular-dependent shading dynamics reliably.

The results showed that while tracking systems substantially reduce direct shading through improved orientation, their advantage is less pronounced for diffuse shading. Nevertheless, both single- and dual-axis trackers consistently outperformed even clean fixed-tilt systems under uniform dust coverage of ~32.7%, indicating the geometric benefits of dynamic

alignment. A techno-economic evaluation further revealed a critical trade-off where tracking maximises absolute energy yield while fixed-tilt systems remain the most cost-effective option due to their lower capital and maintenance requirements.

These insights carry important implications for PV deployment in dusty regions. Dual-axis trackers provide the strongest technical resilience and maximise output. However, their higher costs and operational complexity may limit suitability in resource-constrained settings. Single-axis trackers offer a compromise between yield and cost, while fixed-tilt systems remain the most economically attractive where simplicity and reliability are prioritised.

Future work should incorporate spatially non-uniform soiling, heterogeneous dust properties, and dynamic deposition–cleaning processes to improve real-world predictive accuracy and enable optimised cleaning, tilt, and tracking control strategies in dust-prone environments.

Nomenclature

a	Major axis of elliptical shadow (due to diffuse irradiance)
A_c	Active module area
A_d	Instantaneous diffuse shaded area due to dust
$A_{d,t}$	Total daily diffuse shaded area (integrated from A_d)
A_g	Instantaneous direct shaded area due to dust
$A_{g,t}$	Total daily direct shaded area (integrated from A_g)
b	Minor axis of elliptical shadow; defined as equal to the particle radius (r)
E(t)	Instantaneous PV energy output at time t, adjusted for shading and losses
n	Number of dust particles per unit area
r	Radius of spherical dust particle
T	Module temperature
$T(\theta_i)$	Angular-dependent transmissivity factor
T_{STC}	Standard test condition temperature (25 °C)
α	Temperature coefficient
β	Tilt angle of the PV panel
$\beta(t)$	Time-varying tilt angle for dual-axis tracker
γ	Azimuth angle of the PV panel surface
$\gamma(t)$	Time-varying azimuth angle for dual-axis tracker
γ_s	Solar azimuth angle (sun position)
δ	Solar declination
θ_i	Incidence angle on the tilted PV module
θ_z	Solar zenith angle
ϕ	Geographic latitude
ω	Hour angle

References

[1] Vedulla, G., Geetha, A., & Senthil, R. (2023). Review of Strategies to Mitigate Dust Deposition on Solar Photovoltaic Systems. *Energies*, *16*(1), 109. doi:10.3390/en16010109

[2] Hegedus, S., & Luque, A. (2011). Achievements and Challenges of Solar Electricity from Photovoltaics. In A. Luque & S. Hegedus (Eds.), *Handbook of photovoltaic science and engineering* (pp. 1–38): John Wiley & Sons.

[3] Ammari, N., Mehdi, M., Alami Merrouni, A., El Gallassi, H., Chaabelasri, E., & Ghennioui, A. (2022). Experimental study on the impact of soiling on the modules temperature and performance of two different PV technologies under hot arid climate. *Heliyon*, *8*(11), e11395. doi:10.1016/j.heliyon.2022.e11395

[4] Dahlioui, D., Laarabi, B., & Barhdadi, A. (2019). Investigation of soiling impact on PV modules performance in semi-arid and hyper-arid climates in Morocco. *Energy for Sustainable Development*, *51*, 32–39. doi:10.1016/j.esd.2019.05.001

[5] Lopez-Lorente, J., Polo, J., Martín-Chivelet, N., Norton, M., Livera, A., Makrides, G., & Georghiou, G. E. (2023). Characterizing soiling losses for photovoltaic systems in dry climates: A case study in Cyprus. *Solar Energy*, *255*, 243–256. doi:10.1016/j.solener.2023.03.034

[6] Al Siyabi, I., Al Mayasi, A., Al Shukaili, A., & Khanna, S. (2021). Effect of Soiling on Solar Photovoltaic Performance under Desert Climatic Conditions. *Energies*, *14*(3), 659. doi:10.3390/en14030659

[7] Tummalieh, A., Mittag, M., Reichel, C., Protti, A., & Neuhaus, H. (2025). Holistic Analysis for Mismatch Losses in Photovoltaic Modules: Assessing the Impact of Inhomogeneity from Operational Conditions and Degradation Mechanisms on Power and Yield. *Progress in Photovoltaics: Research and Applications*, *34*(1), 39–59. doi:10.1002/pip.3865

[8] Al Garni, H. Z. (2022). The Impact of Soiling on PV Module Performance in Saudi Arabia. *Energies*, *15*(21), 8033. doi:10.3390/en15218033

[9] Yahya, H. E., Salah, M., Halawa, M. A., Raouf, M., & Ashraf, M. (2025). Energy, exergy, environmental and economic (4E) analysis of PV, CPV and CCPV panels at different climate conditions. *Journal of Al-Azhar University Engineering Sector*, *20*(74), 193–210. doi:10.21608/auej.2024.306080.1688

[10] Kabir, M. S., Niloy, K. M., Rahman, S. M. I., Hossen, M. I., Afrose, S., Mofazzol, M. I. H., & Ahmmed, M. L. (2025). A Novel Method for Detecting Dust Accumulation in Photovoltaic Systems: Evaluating Visible Sunlight Obstruction in Different Dust Levels and AI-based Bird Droppings Detection. *arXiv*, 1–29. doi:10.48550/arXiv.2501.08304

[11] Janiere Silva de Souza, J., Marques de Carvalho, P. C., & Barroso, G. C. (2022). Analysis of the Characteristics and Effects of Soiling Natural Accumulation on Photovoltaic Systems: A Systematic Review of the Literature. *Journal of Solar Energy Engineering, 145*(040801). doi:10.1115/1.4056453

[12] Cang, T. (2025). Comprehensive Exploration of Solar Photovoltaic Technology: Enhancing Efficiency, Integrating Energy Storage, and Addressing Environmental and Economic Challenges. *Applied and Computational Engineering, 123*, 10–16. doi:10.54254/2755-2721/2025.19565

[13] Cormode, D. (2015). Large and Small Photovoltaic Powerplants. (PhD Doctoral Dissertation), The University of Arizona, Department of Physics, Arizona. Retrieved from https://repository.arizona.edu/handle/10150/556863

[14] Massi Pavan, A., Mellit, A., & De Pieri, D. (2011). The effect of soiling on energy production for large-scale photovoltaic plants. *Solar Energy, 85*(5), 1128–1136. doi:10.1016/j.solener.2011.03.006

[15] Fernández, E. F., Chemisana, D., Micheli, L., & Almonacid, F. (2019). Spectral nature of soiling and its impact on multi-junction based concentrator systems. *Solar Energy Materials and Solar Cells, 201*, 110118. doi:10.1016/j.solmat.2019.110118

[16] Chanchangi, Y. N., Ghosh, A., Sundaram, S., & Mallick, T. K. (2020). An analytical indoor experimental study on the effect of soiling on PV, focusing on dust properties and PV surface material. *Solar Energy, 203*, 46–68. doi:10.1016/j.solener.2020.03.089

[17] Sisodia, A. K. (2024). Effect of dust particles size on Photovoltaic module (PV) performance. *International Journal of Science and Research Archive, 13*(2), 3967–3972. doi:10.30574/ijsra.2024.13.2.2653

[18] Martikainen, J., Muñoz, O., Gómez Martín, J. C., Passas Varo, M., Jardiel, T., Peiteado, M., Willame, Y., Neary, L., Becker, T., & Wurm, G. (2025). Database of Martian dust optical properties in the UV-vis-NIR. *Monthly Notices of the Royal Astronomical Society, 537*(2), 1489–1503. doi:10.1093/mnras/staf108

[19] Piedra, P. G., Llanza, L. R., & Moosmüller, H. (2018). Optical losses of photovoltaic modules due to mineral dust deposition: Experimental measurements and theoretical modeling. *Solar Energy, 164*, 160–173. doi:10.1016/j.solener.2018.02.030

[20] Tanesab, J., Parlevliet, D., Whale, J., & Urmee, T. (2019). The effect of dust with different morphologies on the performance degradation of photovoltaic modules. *Sustainable Energy Technologies and Assessments, 31*, 347–354. doi:10.1016/j.seta.2018.12.024

[21] Faeth, G. M., & Köylü, Ü. Ö. (1999). Soot Morphology and Optical Properties in Nonpremixed Turbulent Flame Environments. *Clean Combustion Technologies, 108*(4-6), 207–229. doi:10.1080/00102209508960399

[22] Sharma, S., Malik, P., & Sinha, S. (2024). The impact of soiling on temperature and sustainable solar PV power generation: A detailed analysis. *Renewable Energy, 237*, 121864. doi:10.1016/j.renene.2024.121864

[23] Gedifew, A., & Benor, A. (2025). Evaluating the impact of tilt angles and tracking mechanisms on photovoltaic modules in Ethiopia. *Frontiers in Energy Research, 12:1519725*. doi:10.3389/fenrg.2024.1519725

[24] Mainil, R. I., Rahman, A., Arief, D. S., Mainil, A. K., Hossain, M. A., & Aziz, A. (2025). Performance Comparison of Heat Pipe Photovoltaic/Thermal (HP-PV/T) Wick and Wickless at Different Tilt Angle. *Journal of Advanced Research in Fluid Mechanics and Thermal Sciences, 126*(1), 39–51. doi:10.37934/arfmts.126.1.3951

[25] Oluchi, O. V., Kelechi, D. L., Chukwuemeka, E. V., Anselm, O. C., & Opara, E. K. (2024). Exploring the Ideal Photovoltaic (PV) Tilt Angle Across the Six Geo-Political Zones in Nigeria. *Journal of Electrical Engineering and Electronics Design, 2*(2), 25–30. doi:10.48001/joeeed.2024.2225-30

[26] Dahlioui, D. (2022). Improvement of photovoltaic systems efficiency using innovative, ecological and low cost cleaning techniques. (PhD Thesis), Mohammed V University, Rabat. Retrieved from https://toubkal.imist.ma/handle/123456789/33595

[27] Yunus Khan, T. M., Soudagar, M. E. M., Kanchan, M., Afzal, A., Banapurmath, N. R.,

Akram, N., Mane, S. D., & Shahapurkar, K. (2020). Optimum location and influence of tilt angle on performance of solar PV panels. *Journal of Thermal Analysis and Calorimetry, 141*(1), 511–532. doi:10.1007/s10973-019-09089-5

[28] Babatunde, A. A., Abbasoglu, S., & Senol, M. (2018). Analysis of the impact of dust, tilt angle and orientation on performance of PV Plants. *Renewable and Sustainable Energy Reviews, 90*, 1017–1026. doi:10.1016/j.rser.2018.03.102

[29] Nwokolo, S. C., Obiwulu, A. U., Amadi, S. O., & Ogbulezie, J. C. (2023). Assessing the Impact of Soiling, Tilt Angle, and Solar Radiation on the Performance of Solar PV Systems. *Trends in Renewable Energy, 9*(2), 120–136. doi:10.17737/tre.2023.9.2.00156

[30] Feteh, M. (2021). Optimizing the Design of PV Plants for the Cases of a Fixed Tilt Angle and a Solar Tracker. (MSc Master's Thesis), Politecnico di Milano, Retrieved from https://hdl.handle.net/10589/173701

[31] Li, G., Chen, Y., Yu, Y., Tang, R., & Mawire, A. (2019). Performance and design optimization of single-axis multi-position sun-tracking PV panels. *Journal of Renewable and Sustainable Energy, 11*(6), 063701. doi:10.1063/1.5115976

[32] Chen, Y. B., Tang, J. J., Li, G. H., & Yu, Y. M. (2019). Photovoltaic performance of one axis multiple-position sun-tracked PV panels. *IOP Conference Series: Earth and Environmental Science, 354*(1), 012128. doi:10.1088/1755-1315/354/1/012128

[33] Barbón, A., Martínez-Suárez, J., Bayón, L., & Bayón-Cueli, C. (2025). Photovoltaic Power Plants with Horizontal Single-Axis Trackers: Influence of the Movement Limit on Incident Solar Irradiance. *Applied Sciences, 15*(3), 1175. doi:10.3390/app15031175

[34] Uchaipichat, N., Wibunsin, C., Chokjulanon, K., & Tanthanuch, N. (2025). Computer vision-based sun tracking control for optimizing photovoltaic power generation. *International Journal of Electrical and Computer Engineering (IJECE), 15*(2), 1251–1261. doi:10.11591/ijece.v15i2.pp1251-1261

[35] Alexandru, C. (2019). Optimal design of the dual-axis tracking system used for a PV string platform. *Journal of Renewable and Sustainable Energy, 11*(4), 043501. doi:10.1063/1.5109390

[36] Abdullah, H. K., & Abdulkarim, P. M. (2023). A Design Model And Comparison of Fixed And Tracking Photovoltaic Systems for A Single-family House in Erbil, Iraq. *The Journal of Duhok University, 26*(2), 515–532. doi:10.26682/csjuod.2023.26.2.47

[37] Abdelsalam, M. A. M., Ahmad, F. F., Hamid, A.-K., Ghenai, C., Rejeb, O., Alchadirchy, M., Obaid, W., & Assad, M. E. H. (2021). Experimental study of the impact of dust on azimuth tracking solar PV in Sharjah. *International Journal of Electrical and Computer Engineering (IJECE), 11*(5), 3671–3681. doi:10.11591/ijece.v11i5.pp3671-3681

[38] Pouladian-Kari, A., Eslami, S., Tadjik, A., Kirchner, L., Pouladian-Kari, R., & Golshanfard, A. (2022). A novel solution for addressing the problem of soiling and improving performance of PV solar systems. *Solar Energy, 241*, 315–326. doi:10.1016/j.solener.2022.06.012

[39] Mamodiya, U., Kishor, I., Garine, R., Ganguly, P., & Naik, N. (2025). Artificial intelligence based hybrid solar energy systems with smart materials and adaptive photovoltaics for sustainable power generation. *Scientific Reports, 15:17370*. doi:10.1038/s41598-025-01788-4

[40] Guo, B., & Javed, W. (2024). Effect of incidence angle on PV soiling loss. *Solar Energy, 269*, 112298. doi:10.1016/j.solener.2023.112298

[41] Chala, G. T., Sulaiman, S. A., & Chen, X. (2025). A Study on the Performance of Soiled Solar Photovoltaic Panels at Different Tilt Angles in Al Seeb, Oman. *Energies, 18*(2), 301. doi:10.3390/en18020301

[42] Tuomiranta, A. (2014). Performance Modelling of Photovoltaic Power Stations for an Interactive Solar Energy Atlas of the Arabian Peninsula. (MSc Thesis Master's Thesis), Aalto University, Abu Dhabi. Retrieved from https://aaltodoc.aalto.fi/handle/123456789/14697

[43] Pagani, V. H., Los, N. A., Maidana, W., Leitão, P., Casaro, M. M., & Nascimento, C. B. *Soiling Monitoring Modelling for Photovoltaic System*. Paper presented at the CONTROLO 2020: Lecture Notes in Electrical Engineering, Bragança, Portugal. https://link.springer.com/content/pdf/10.1007%2F978-3-030-58653-9_57.pdf

[44] Pop, T., Buzduga, C., Pentiuc, R. D., Ifrim, V. C., & Ungureanu, C. (2022). Mathematical modeling in MATLAB of a photovoltaic panel. *IOP Conference Series: Materials Science and Engineering, 1256*(1), 012037. doi:10.1088/1757-899X/1256/1/012037

[45] Willers, G., Sakarapunthip, N., Ilse, K., Chuangchote, S., & Gottschalg, R. (2025). Impact of Different Types of Dust on Solar Glass

Transmittance and PV Module Performance. *Progress in Photovoltaics: Research and Applications, 33*(8), 844–853. doi:10.1002/pip.3930

[46] Boyle, L., Flinchpaugh, H., & Hannigan, M. P. (2015). Natural soiling of photovoltaic cover plates and the impact on transmission. *Renewable Energy*, *77*, 166–173. doi:10.1016/j.renene.2014.12.006

[47] Diop, D., Drame, M. S., Diallo, M., Malec, D., Mary, D., & Guillot, P. (2020). Modelling of Photovoltaic Modules Optical Losses Due to Saharan Dust Deposition in Dakar, Senegal, West Africa. *Smart Grid and Renewable Energy*, *11*(7), 89–102. doi:10.4236/sgre.2020.117007

[48] Thungsuk, N., Tanaram, T., Chaithanakulwat, A., Savangboon, T., Songruk, A., Mungkung, N., Maneepen, T., Arunrungrusmi, S., Poonthong, W., Kasayapanand, N., Nilwhut, S., Kinoshita, H., & Yuji, T. (2023). Performance Analysis of Solar Tracking Systems by Five-Position Angles with a Single Axis and Dual Axis. *Energies*, *16*(16), 5869. doi:10.3390/en16165869